Investigation on Aerodynamic Interaction of Tandem Tilt-Wing and Multi-rotor in Transition Condition

DENG Jinghui, *YUAN Mingchuan**, *HUANG Shuilin*, *SUN Huixun*, *ZHANG Zihan*

National Key Laboratory of Helicopter Aeromechanics, China Helicopter Research and Development Institute, Jingdezhen 333000, P. R. China

(Received 22 January 2025; revised 25 June 2025; accepted 10 October 2025)

Abstract: The complex aerodynamic interaction between tandem tilt-wing and multi-rotor directly affects the wing surface flow and rotor thrust, making it a critical factor during the tilt transition process of this configuration of rotorcraft. The aerodynamic interaction of tandem tilt-wing and multi-rotor is investigated based on the CFD method. The aerodynamic effect of multi tilt-rotor is simulated as virtual disk modeling by adding source terms to the Navier-Stokes equations, effectively reducing the calculation time while maintaining the accuracy of aerodynamic interaction calculations. Aerodynamic forces and flow field characteristics of the tandem tilt-wing and multi-rotor under different tilt angles are compared between cases with and without aerodynamic interaction. Furthermore, the differences in aerodynamic forces between dynamic tilt transition and fixed-angle conditions were compared. The results show that the aerodynamic interaction of multi-rotor obviously increases the lift of front tilt-wing at different tilt angles, the wing lift under interaction is increased by more than 40% compared with isolated wing at tilt angle of 15° for the computation in this paper, which is related to the increase of wing flow velocity and the suppression of flow separation caused by multi-rotor; the wing blocking effect will increase rotor thrust, especially near the tilt angles of 30° and 45°; the increases of rear wing lift and rear rotor thrust under aerodynamic interaction are not significant because of suppression by the front wing's downwash; the unsteady effects during dynamic tilting have a relatively minor impact on aerodynamic interaction, with the aerodynamic forces on the rotors and wings during the dynamic tilting process showing little difference from those under corresponding fixed tilt angles.

Key words: aerodynamic interaction; tandem; tilt-wing; multi tilt-rotors; transition condition

CLC number: V211.52 **Document code:** A **Article ID:** 1005-1120(2026)01-0001-14

0 Introduction

The flight speed of helicopters is limited by aerodynamic phenomena such as advancing-side compressibility and rearward-side dynamic stall, which occur in helicopter rotor during high-speed flight[1-2]. These factors make it difficult for the maximum flight speed of helicopters to exceed 300 km/h. By tilting rotor to a propeller mode, the limiting factors mentioned above can be significantly weakened because the rotor operates in an axial flow condition. Therefore, the tilt-rotor concept is one of the primary directions for achieving high speed development in rotorcraft. In recent years, rotorcraft configurations combining distributed tilt multi-rotor and tandem tilt-wing have gradually attracted the attention of researchers. For example, the "GL10" concept[3] developed by NASA Langley Research Center and the "Vahana" unmanned rotorcraft[4] designed by Airbus adopt this configuration, as shown in Fig.1. These designs are considered to be among the most important options for future urban air transport.

*Corresponding author, E-mail address: yuanmingchuande@126.com.

How to cite this article: DENG Jinghui, YUAN Mingchuan, HUANG Shuilin, et al. Investigation on aerodynamic interaction of tandem tilt-wing and multi-rotor in transition condition[J]. Transactions of Nanjing University of Aeronautics and Astronautics, 2026, 43(1): 1-14.

http://dx.doi.org/10.16356/j.1005-1120.2026.01.001

(a) GL10[3] (b) Vahana[4]

Fig.1 GL10[3] and Vahana[4]

Aircraft with multi-rotor combined with tandem tilt-wing configuration, such as Vahana, have serious aerodynamic interaction problems during flight. There is not only interaction between rotors and their mounted wings, but also mutual interaction between front and rear wings or rotors. Especially in the transition condition, the rotors are tilted together with the wings, which exacerbates the complexity of aerodynamic interaction. In transition condition, the wing angle is much larger than the stall angle of attack, the aerodynamic interaction has a great impact on tilt-wing flow separation. Understanding the rotor and wing aerodynamic characteristics under mutual interaction is a key factor for the aircraft configuration to successfully achieve transition conversion.

Focusing on aerodynamic interaction between rotor and wing in transition condition, previous investigation primarily concentrated on tilt-rotor aircraft configurations like the V-22[5-9]. Appleton et al.[10] examined the influence of aerodynamic interactions among the rotor, wing and horizontal tail on transition corridor boundary using a reduced order aerodynamic model. Wu et al.[11] employed the overset mesh method combined with Reynolds-Averaged Navier-Stokes (RANS) equations to simulate the aerodynamic characteristics of tilt-rotor aircraft in continuous transition state, and compared the influence of transition time, rotor control and other factors on aerodynamic interaction of rotor and wing during transition. Wu et al.[12] utilized CFD to analyze both quasi-steady and transient aerodynamic interaction between tilt-rotor and wing in transition state, treating the rotor as a momentum source term added on the right side of the Navier-Stokes equations for aerodynamic analysis. However, research on aerodynamic interaction of tandem tilt-wing and distributed multi-rotor remains limited. In recent years, Joby Aviation has been devoted to the development of Joby S4 multi-tiltrotor aircraft. Refs.[13-16] conducted a large amount of research on rotor aerodynamic design and acoustic characteristics for this aircraft, but relatively few studies have focused on aerodynamic interaction characteristics. Perez et al.[17-18] analyzed the aerodynamic characteristics of tilt-wing and multi-rotor using both mid-fidelity virtual disk modeling and high-fidelity blade-resolved CFD methods. However, their analysis of aerodynamic interaction between front and rear wings and rotors was insufficient.

Based on the above research background, this paper investigates the aerodynamic interactions of tandem tilt-wing and distributed multi-rotor in transition conditions. The virtual disk modeling CFD method based on RANS equations is employed for numerical calculations. The study compares the effects of aerodynamic interactions on rotor and wing forces at different tilt angles, analyzes the corresponding flow field changes, and draws several conclusions.

1 Calculation Method and Validation

1.1 Method description

The virtual disk modeling CFD method is used to calculate and analyze the aerodynamic interaction. The aerodynamic action of rotors is simplified as multiple virtual disks by adding source term to the Navier-Stokes equations, ignoring detailed aerodynamic characteristics of the rotor blades. The virtual disk modeling CFD method has high computational efficiency and can accurately simulate the aerodynamic interaction force and flow field between rotors and wings. This method has good applicability in the aerodynamic analysis of the rotor aircraft[19-23].

The governing equation adopts RANS equations, and the effect of rotor on flow field is simulated by adding momentum source on the right side of the RANS equations. The governing equation can be written in an integral form as

$$\frac{\partial}{\partial t}\iiint \boldsymbol{W}\mathrm{d}\Omega+\iint(\boldsymbol{F}_{\mathrm{c}}-\boldsymbol{F}_{\mathrm{v}})\boldsymbol{n}\mathrm{d}S=\boldsymbol{Q} \tag{1}$$

where Ω is the volume of the control unit in the flow field space; t the time; $\boldsymbol{W}$ the vector of conserved quantities; $\boldsymbol{Q}$ the momentum source term simulating the rotor aerodynamic effect; $\boldsymbol{F}_v$ the vectors of viscous fluxes; and $\boldsymbol{F}_c$ the vectors of inviscid fluxes. They are given by

$$\boldsymbol{W}=\begin{bmatrix}\rho\\ \rho u\\ \rho v\\ \rho w\\ \rho E\end{bmatrix},\boldsymbol{F}_c=\begin{bmatrix}\rho(V-V_e)\\ \rho u(V-V_e)+pi\\ \rho v(V-V_e)+pj\\ \rho w(V-V_e)+pk\\ \rho h(V-V_e)+pV_e\end{bmatrix} \tag{2}$$

$$\boldsymbol{F}_v=\begin{bmatrix}0\\ \tau_{xx}i+\tau_{xy}j+\tau_{xz}k\\ \tau_{yx}i+\tau_{yy}j+\tau_{yz}k\\ \tau_{zx}i+\tau_{zy}j+\tau_{zz}k\\ \Theta_x i+\Theta_y j+\Theta_z k\end{bmatrix},\boldsymbol{Q}=\begin{bmatrix}0\\ S_x\\ S_y\\ S_z\\ 0\end{bmatrix} \tag{3}$$

where ρ is the air density; p the air pressure; $V=[u\ v\ w]^T$ the absolute velocity in the flow field; E the total energy per unit mass; h the total enthalpy; and V_e the motion speed of the grid cell. S_x, S_y, S_z are the components of the momentum source term in all three directions.

The finite volume method with Roe MUSCL upwind scheme is used to discretize the fluid domain. The shear stress transport (SST) k-ω model, which has been widely validated to various rotor flow simulations[24-27], is used in the present computation to model the turbulence effect in the interaction flow. The calculation ignored the influence of the boundary layer transition, and the flow assumed to be fully turbulent. In the unsteady calculation, the implicit LU-SGS method is used for time discretization, and the dual-time marching method is used with 20 inner iterations in each physical time step.

The rotor is modeled as a virtual disk that produces momentum source, and the periodic actions of rotor are simplified to "quasi-steady" flow through time averaging method in the virtual disk modeling. The disk is discretized into many small elements along the radial and circumferential directions. The radial discretization helps to simulate the aerodynamic influence due to variation of rotor blade shape, and the circumferential discretization helps to simulate the flow variation at different azimuths during the rotor rotation. The lift and drag force of different disk elements are calculated by the blade element method which uses the aerodynamic shape and motion of blade, the variation of the surrounding flow with the rotating azimuth angle, and the aerodynamic characteristics of blade airfoil as calculation input. The aerodynamic characteristics of blade airfoil are obtained by interpolation from the C81 table file which includes lift, drag and moment coefficients of different Mach numbers and attack angles of airfoil.

1.2 Validation of calculation method

In order to verify the validity and accuracy of the calculation method, an example of rotor and fuselage aerodynamic interaction experimental results is selected to compare with the calculation results. The test was carried out in Glenn L. Martin wind tunnel of the University of Maryland[28-29]. In the test, the rotor model diameter was 1.65 m, the fuselage length was 1.94 m, and the aerodynamic force of the rotor and fuselage and the pressure coefficient of the fuselage surface were obtained. Fig.2 shows the comparison with experimental results of the rotor aerodynamic coefficient under aerodynamic interaction. Fig.3 shows the comparison with the experimental results of fuselage pressure coefficient with and without aerodynamic interaction. According to the comparison results, it can be seen that the calculation and test results show a good agreement, and the change of fuselage pressure coefficient caused by rotor interaction has been accurately simulated in the calculation. This shows that the calculation method adopted in this paper can be used to calculate and analyze the aerodynamic interaction characteristics of the rotorcraft effectively.

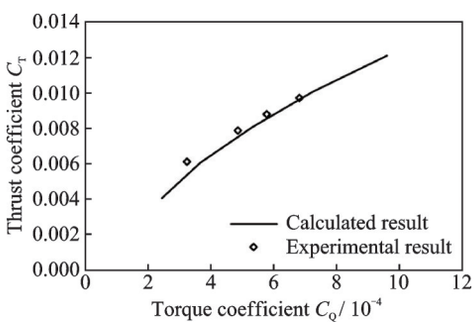

Fig.2 Comparison of the calculated and experimental results of rotor aerodynamic coefficient

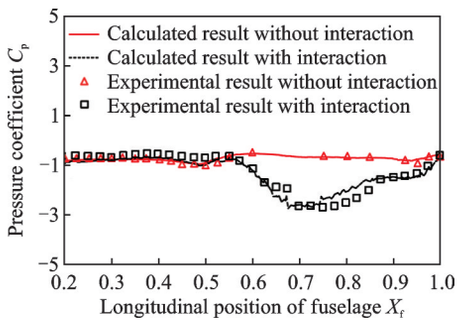

Fig.3 Comparison of the calculated and experimental results of fuselage pressure coefficient

2 Results and Analysis

This section analyzes the influence of aerodynamic interaction on the aerodynamic characteristics of different components under tilting condition, including front rotors, front wing, rear rotors and rear wing. Firstly, the aircraft model, flight conditions, and computational gird used in the calculation are introduced, and then the aerodynamic force and flow field results with and without interaction are compared.

2.1 Calculation model

Fig.4 is a schematic diagram of the multi tilt-rotor aircraft analyzed in this paper. The aircraft adopts tandem tilt-wing combined with distributed multi-rotor configuration, with a total of 12 rotors. In the following, rotors 1, 7, 6, 12 are referred to as outboard rotors; rotors 2, 8, 5, 11 are referred to as middle rotors; rotors 3, 4, 9, 10 are referred to as inboard rotors. The wings and rotors are vertical in helicopter mode, and transition to propeller aircraft mode by tilting the wings and rotors to horizontal direction together. Fig.4 also shows the relative position between rotors and wings. In present analysis, the calculation is mainly focused on aerodynamic interaction between the rotors and the mounted wing as well as interaction between front and rear wings or rotors, and the influence of the fuselage and nacelle is ignored.

In the calculation model, the rotor diameter is 1.8 m, the rotor blade number is 4, and airfoils used by rotor blade consist of NACA4412, NACA2409 and NACA1406. The solidity of the rotor mounted on the tip of the wing and the inside of the wing is 0.12 and 0.17, respectively. The rotation direction of the rotors on the left side of the front wing is clockwise, while left side of the rear wing is counterclockwise, and the rotation direction of the rotors on both sides of the symmetry plane of the aircraft is opposite. The wings have a trapezoidal plane shape and the airfoil used is Eppler 748.

2.2 Calculation conditions

In the transition condition of the multi-tilt-rotor aircraft, the tilt angle of the front and rear wings remains the same, and the rotor control consists of collective pitch angle only. Fig.5 shows the transition corridor of the aircraft, in which several flight conditions with different tilt angles are selected for present numerical calculation. The transition corridor and control strategy at different tilt angles of the aircraft were obtained by flight dynamic analysis with the Flightlab software in the early stage. This paper mainly analyzes the aerodynamic interaction characteristics, and will not introduce the detailed analysis of flight dynamic characteristics. Table 1 gives detailed parameters of different calculation conditions, in which, V is the flight velocity; α_s the tilt angle of wing and rotor; ω the rotor frequency; α_{ff} the front flap angle; α_{fr} the rear flap angle; θ_{In} the inboard rotor collective pitch; θ_{Mid} the middle rotor collective pitch; and θ_{Out} the outboard rotor collective pitch.

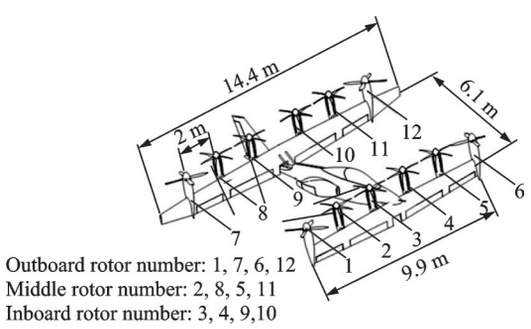

Fig.4 Schematic diagram of the multi tilt-rotor aircraft

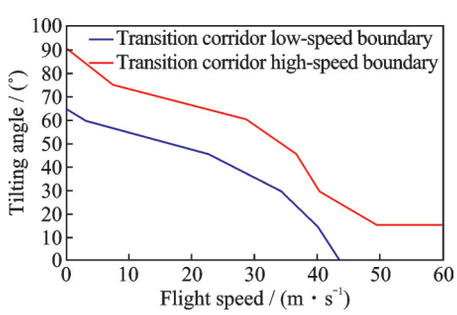

Fig.5 Transition corridor adopted in the calculation

Table 1 Calculation conditions

Case	V/(m•s^{-1})	α_s/(°)	ω/(rad•s^{-1})	α_{ff}/(°)	α_{fr}/(°)	θ_{In}/(°)	θ_{Mid}/(°)	θ_{Out}/(°)
1	58.68	0	260	30.00	25.00	17.54	17.54	16.00
2	40.56	15	260	20.00	0.00	17.54	17.54	12.50
3	38.89	30	260	20.00	0.00	17.54	17.54	9.10
4	31.07	45	260	20.00	0.00	17.54	17.54	5.73
5	19.85	60	260	10.00	0.00	17.54	17.54	8.48
6	2.78	75	260	0.00	0.00	17.54	17.54	11.61

2.3 Calculation settings

The right half side of the aircraft is modeled base on symmetric boundary conditions during CFD calculation to improve computational efficiency. In the calculation, the grid near the rotor disk is refined to capture more accurate rotor inflow, and the prism layer grid is used near the wing surface to better simulate the boundary layer flow. The total number of meshes in the computational domain is 7.97 million, and Fig.6 shows a schematic diagram of the mesh at the longitudinal slice. The number of radial discrete elements of rotor disk is 30, and the number of circumferential elements is 36.

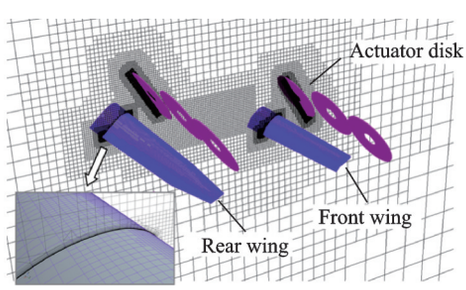

Fig.6 Diagram of computation grid at the longitudinal slice

2.4 Influence of aerodynamic interaction on front and rear wings

The front and rear multi-rotors, as well as the front and rear wings, exhibit complex mutual aerodynamic interactions. As the wake generated by the wings and rotors moves rearward with the free stream, the front wing and front rotors are primarily influenced by their mutual aerodynamic interactions. In contrast, the rear wing and rear rotors are affected not only by their mutual interactions but also by the aerodynamic interactions of the front rotors and front wing. This section focuses on analyzing the variations in aerodynamic forces and the underlying flow mechanisms of the front and rear wings under these complex interactions. The next section primarily examines the changes in aerodynamic forces and flow mechanisms of the front and rear rotors under aerodynamic interactions.

Figs.7, 8 show the comparison of front wing and rear wing lift with and without aerodynamic interaction, respectively. It can be seen that, in most cases of tilt angles between 0°and 60°, aerodynamic interaction significantly increases the lift of the front wing, and the lift increment of the front wing under interaction can reach more than 40% when the tilt angle is 15°. For the rear wing, the lift increment caused by aerodynamic interaction is obviously smaller than that of the front wing at tilt angles of 0° and 15°, even becomes a significant negative value at tilt angle of 0°, while after tilt angle of 30° the lift increment of the rear wing caused by aerodynamic interaction is higher than that of the front wing.

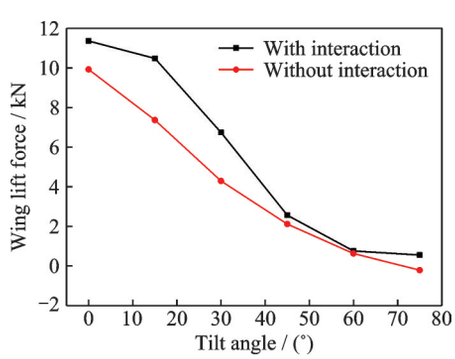

Fig.7 Lift variation (Front wing)

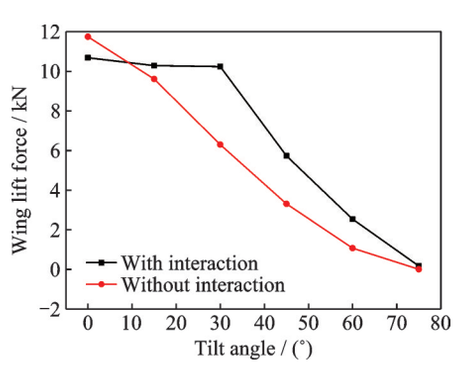

Fig.8 Lift variation (Rear wing)

Fig.9 shows the vorticity contours on a series of planes parallel to rotor disk at tilt angles of 0°, 15° and 30° under full interaction of tandem tilt-wing and multi-rotor. It can be seen that the front and rear wings are significantly affected by the wake of multi-rotor, and the vorticity magnitude and the position relative to the wings of the rotor wake are changed along with tilt angles. The pressure contours and streamlines on longitudinal plane around the front wing at tilt angles of 0°, 15° and 30° are analyzed in Figs.10—12. The longitudinal plane is located at 60% span position to symmetry plane (approximately behind the middle front rotor). For the tilt angle of 0°, it can be clearly seen that the high-pressure area on the lower wing surface and the low-pressure area on the upper wing surface are more obvious with aerodynamic interaction than those without interaction. At the same time, the aerodynamic interaction does not change the direction of the streamline around the wing, and there is local flow separation caused by trailing edge flap deflection in both with and without interaction. This indicates that the increase of flow velocity caused by rotor slipstream interaction at tilt angle of 0° is the main factor for wing lift increase. For the tilt angle of 15°, the obvious aerodynamic separation basically occurs on the upper wing surface for condition without interaction, resulting in the wing stall. However, rotor interaction makes the streamline direction around the wing deflect downward, reducing the flow separation. This shows that the wing lift increase is due to a combination of delayed wing stall and increased flow velocity caused by rotor interaction. For the tilt angle of 30°, the isolate wing is in deep stall, while the improvement of wing stall is more obvious with rotor interaction. Therefore, the increase of flow velocity caused by multi-rotor aerodynamic interaction is the main factor for the wing lift increase at small tilt angles when there is no obvious flow separation, while at large tilt angles the rotor slipstream improves the wing flow separation, which leads to the extra increase of wing lift.

For the rear wing the induced velocity of the front wing and the slipstream interaction of the front rotors will also affect its aerodynamic characteristics besides the rear rotors interaction mounted on it. At small tilt angles, the front wing lift is at a high level, and the generated downward induced velocity will significantly reduce the rear wing lift. This is the main reason for the rear wing lift reduction caused by aerodynamic interaction at tilt angle of 0° in Fig.8. At large tilt angles, the slipstream interaction of the front rotor will further improve the flow separation of the rear wing, which will lead to the rear wing generate larger lift increment under aerodynamic interaction.

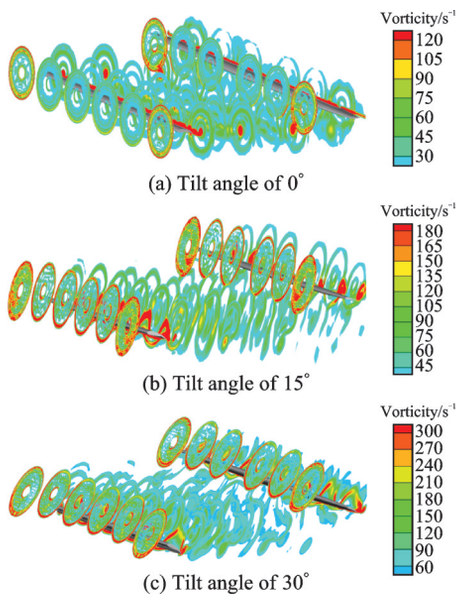

Fig.9 Vorticity contours on a series of planes parallel to rotor disk at different tilt angles

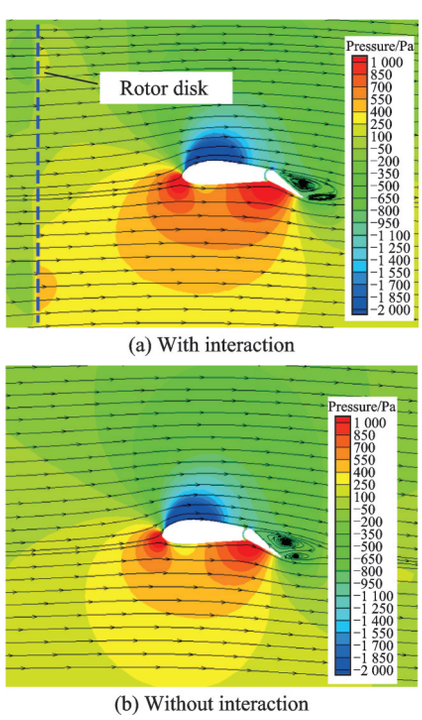

Fig.10 Pressure contour and streamlines around wing section (Tilt angle of 0°, comparison with isolate wing)

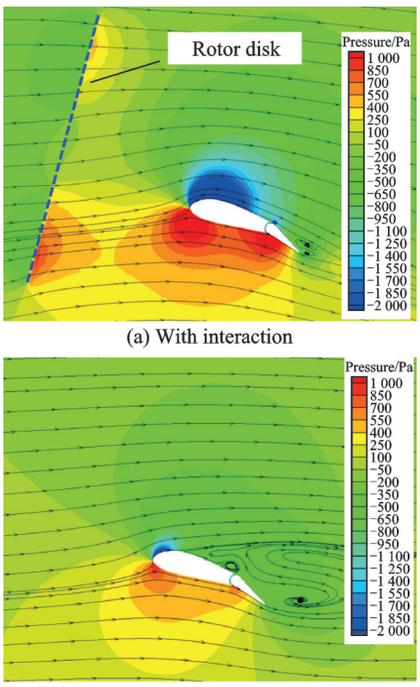

(a) With interaction

(b) Without interaction

Fig.11 Pressure contour and streamlines around wing section (Tilt angle of 15°, comparison with isolate wing)

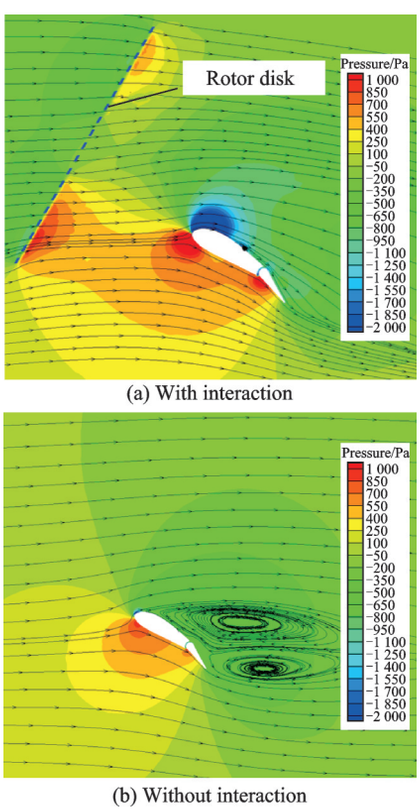

(a) With interaction

(b) Without interaction

Fig.12 Pressure contour and streamlines around wing section (Tilt angle of 30°, comparison with isolate wing)

Figs.13, 14 show the comparison of front wing and rear wing drag with and without aerodynamic interaction, respectively. It can be seen that, aerodynamic interaction leads to the drag of both the front and rear wings increase significantly at most tilt angles, and the drag of the rear wing increases more obviously. The drag increase on the front wing is attributed to the downwash flow deflection caused by the tilting rotor slipstream interaction, which generates a rearward horizontal force component from the wing lift originally perpendicular to the flow direction. The rear wing, while subjected to interaction from the rear rotor slipstream, is also affected by the combined influence of the front wing and front rotors, resulting in a more obvious drag increase. Additionally, the increase in flow velocity induced by rotor aerodynamic interaction further contributes to the drag increase to some extent.

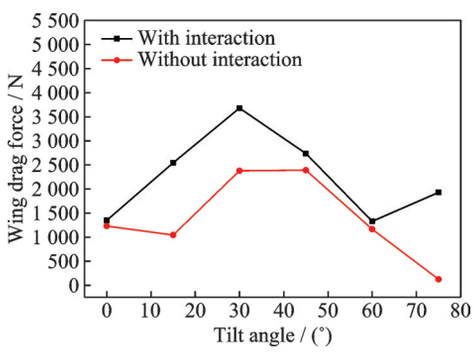

Fig.13 Drag variation (Front wing)

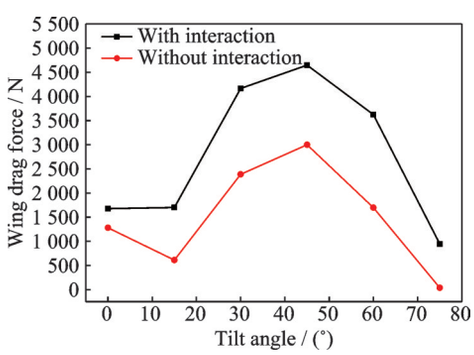

Fig.14 Drag variation (Rear wing)

A comparative analysis of the wing lift-to-drag ratio is further conducted at the tilt angle of 0°. At this angle, the lift-to-drag ratio of the front wing increases by 4.3%, while that of the rear wing decreases by approximately 30%. The improvement in the front wing's lift-to-drag ratio is attributed to an increase in lift under the aerodynamic influence of the front rotors, without a significant increase in drag. In contrast, the reduction in the rear wing's lift-to-drag ratio results from lift decrease and drag increase induced by the downwash interaction from

the front wing. The front wing drag increase caused by aerodynamic interaction at tilt angle of 0° is not obvious, which is related to the aerodynamic interaction of wing tip rotor. Fig.15 shows a comparison of the vorticity contour of lateral section near the front wing tip with and without interaction. It can be seen that there is an obvious concentrated vortex at the wing tip without interaction, which will generate obvious induced velocity and thus cause induced drag. However, when there is interaction, the rotation direction of the front wing tip rotor is opposite to the wing tip vortex direction, and the rotating flow of the rotor will cause reverse vorticity, which weakens the wing tip vortex induction effect and thus reduces the induced drag.

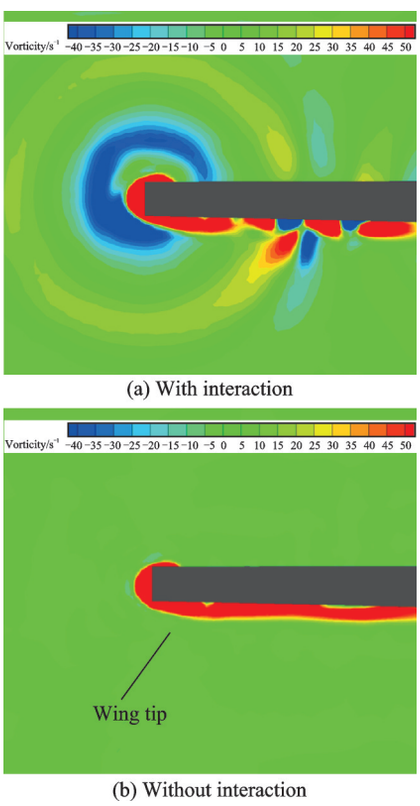

(a) With interaction

(b) Without interaction

Fig.15 Vorticity contour on lateral plane near the front wing tip (Tilt angle of 0°, comparison with isolate wing)

2.5 Influence of aerodynamic interaction on front and rear rotors

Figs.16—18 show the variation of thrust coefficients for three front rotors located on the outboard, middle and inboard sides at different tilt angles. It can be seen that, the thrust coefficient variation trend of outboard rotor is quite different from that of middle and inboard rotors, which is mainly related to the difference of collective pitch angle variation during transition between them. Comparing the lift coefficient of the outboard rotor with and without interaction, it can be found that the rotor thrust is higher with interaction, especially for tilt angles of 30° and 45°. The wing interaction increases the inboard rotor thrust by 5.6% at tilt angle of 45°. The reason of rotor thrust increase is that the wing will block the rotor flow, which increases rotor thrust like the ground effect. For the middle and inboard rotors, aerodynamic interaction also increases rotor thrust at tilt angle up to 45°, but aerodynamic interaction decreases rotor thrust at tilt angles of 60° and 75°. The decrease in middle and inboard rotor thrusts is mainly due to the effect of downward induced velocity generated by the surrounding rotor wake, while this interaction has a relatively weak effect on the outboard rotor. Fig.19 shows the variation of torque coefficient for the outboard rotor with and without interaction. It can be found that the aerodynamic interaction also causes an increase in the rotor torque coefficient, but the increase is smaller than the rotor thrust coefficient.

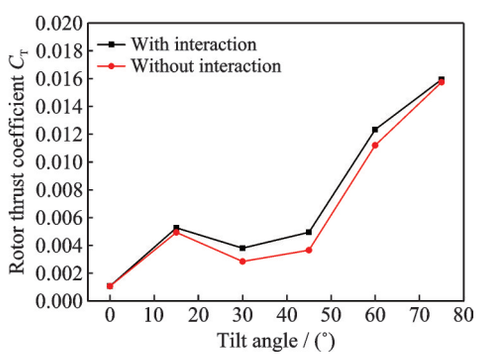

Fig.16 Thrust coefficient variation of outboard rotor of the front rotors

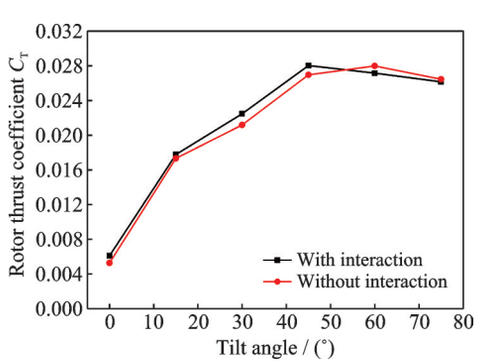

Fig.17 Thrust coefficient variation of middle rotor of the front rotors

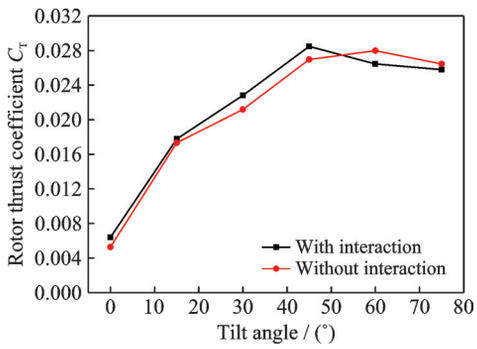

Fig.18 Thrust coefficient variation of inboard rotor of the front rotors

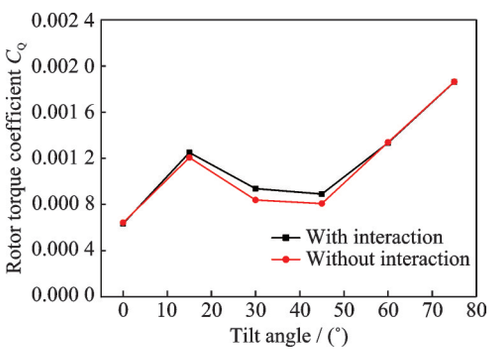

Fig.19 Torque coefficient variation of outboard rotor of the front rotors

Fig.20 shows the vorticity contours on a series of planes perpendicular to rotor disk at tilt angles of 75° and 45°. It can be seen that the interactions of the wings and the wake of multi-rotor at different tilt angles are quite different. The interaction is weak at tilt angle of 75°, but the wing has significant interaction on the wake bottom boundary at tilt angle of 45°. Figs.21, 22 show the comparison of pressure contour and streamlines on longitudinal plane around front rotor with and without wing interaction at tilt angles of 75° and 45°, respectively. It can be

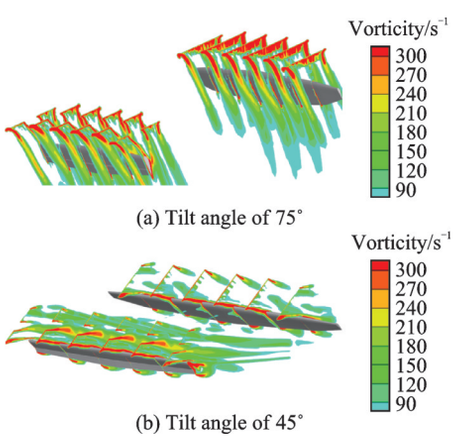

Fig.20 Vorticity contours on a series of planes perpendicular to rotor disk at different tilt angles

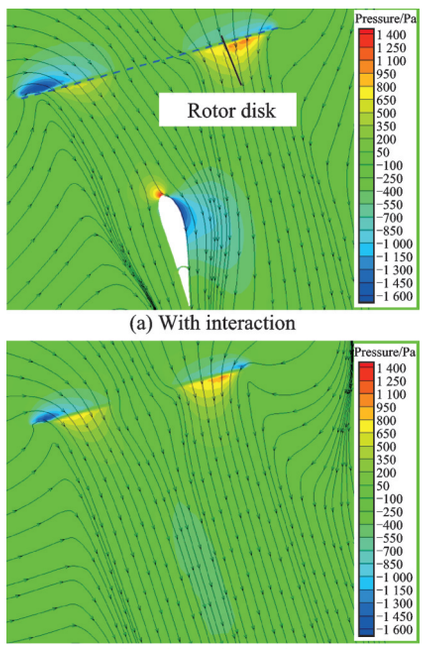

Fig.21 Pressure contour and streamlines on longitudinal plane around middle rotor of the front rotors (Tilt angle of 75°, comparison with isolate rotor)

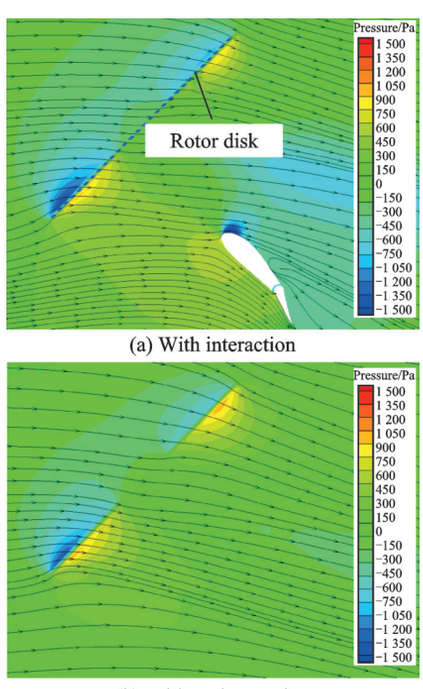

Fig.22 Pressure contour and streamlines on longitudinal plane around middle rotor of the front rotors(Tilt angle of 45°, comparison with isolate rotor)

seen that, when the tilt angle is 75°, the cross-sectional area of the tilt-wing in the rotor downwash flow is very small, resulting in quite weak blocking effect. When the tilt angle is 45°, due to the influence of the separated flow on the upper surface of

the wing, more blocking effect will be caused to the rotor, which will further increase the rotor thrust. This is why the aerodynamic interaction lead to a greater increase in rotor lift at tilt angle of 45°.

Figs.23—25 show the variation of thrust coefficients for rear rotors with and without aerodynamic interaction. It can be seen that, the aerodynamic interaction does not significantly increase the lift of the rear rotors, and even slightly decreases it at tilt angles of 0° and 15° for middle rotor and inboard rotor, which is inconsistent with the influence of aerodynamic interaction on the front rotor. This is mainly due to the complex influence of multiple aerodynamic interactions caused by the front wing and the front rotor as well as the rear wing's blocking effect. At small tilt angles such as 0° and 15°, the rear rotor will be affected by both axial induced velocity and circumferential swirling flow of the front rotor. The axial inflow will reduce the effective angle of attack of the rear rotor, thus reducing the rotor pull, while the effect of circumferential swirl is related to the rotation direction. At moderate tilt angles around 45°, the induced velocity of the forward wing and the slipstream of the forward rotor have an downward inflow component perpendicular to the rear rotor disk, which also causes a decrease in rear rotor lift. By comparing Fig.24 and Fig.25, it can be seen that the thrust coefficient curves of middle and inboard rotors without interaction are the same due to adopting the same collective pitch at different tilt angles, and the thrust coefficient curves of middle and inboard rotors with interaction are somewhat different due to the interaction changing their aerodynamic environment.

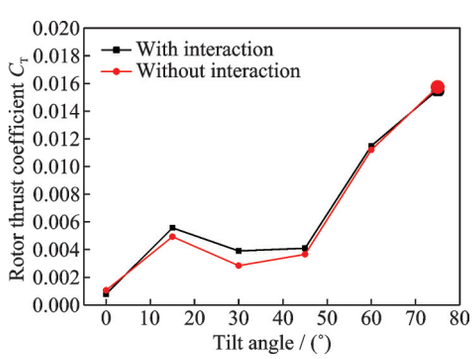

Fig.23 Thrust coefficient variation of outboard rotor of the rear rotors

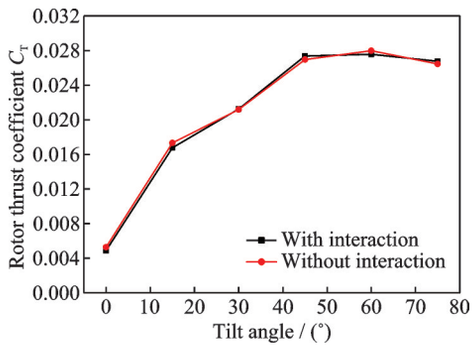

Fig.24 Thrust coefficient variation of middle rotor of the rear rotors

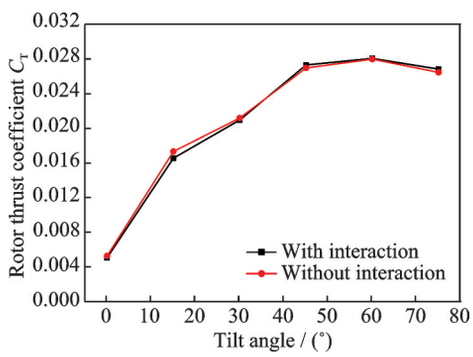

Fig.25 Thrust coefficient variation of inboard rotor of the rear rotors

Fig.26 shows the pressure contour and streamlines on longitudinal plane of the front and rear rotors with aerodynamic interaction at tilt angle of 0°. It can be seen that, there is a slight downward deflection in the inflow direction of the rear rotor compared to the front rotor, which is mainly affected by the induced velocity of the front wing. Fig.27 shows a comparison of inflow velocity values for different vertical positions at 0.15R ahead of the front and rear rotor. It can be seen that the inflow velocity in the lower half of the rear rotor is significantly higher than that in the front rotor, mainly due to the aerodynamic interaction of the front rotor located below the rear rotor, which decreases the thrust of rear rotor. Fig.28 shows the pressure contour and streamlines on longitudinal plane at tilt angle of 45°. It shows that, the inflow velocity direction of rear rotor is deflected downward due to the aerodynamic interaction of front rotor and wing, resulting in an inflow component perpendicular to the rotor disk. These flow field results are in good agreement with the rear rotor aerodynamic force changes in Figs.23—25.

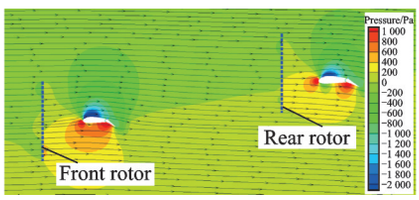

Fig.26 Pressure contour and streamlines on longitudinal plane of front and rear rotor (Tilt angle of 0°, 60% span position)

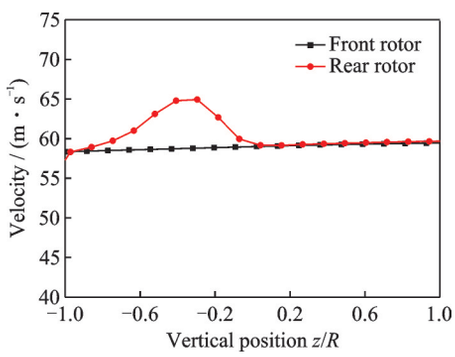

Fig.27 Comparison of rotor inflow velocity in front of rotor

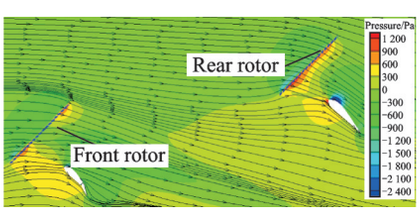

Fig.28 Pressure contour and streamlines on longitudinal plane of front and rear rotor (Tilt angle of 45°, 60% span position)

2.6 Comparison of unsteady and quasi-steady results of transition condition

The aerodynamic characteristics of different tilt angles are calculated by quasi-steady method in the previous chapters, ignoring the unsteady effect of continuous dynamic transition. So, the aerodynamic force in transition process is calculated using unsteady method in this section to compare with the quasi-steady result. The method of overset mesh combined with local coordinate system is used to simulate the tilting and horizontal motion of the wings and rotors in the dynamic transition calculation. The overset mesh includes background mesh, wing mesh and rotor disk mesh, and the linear interpolation is used to transfer the flow field data between different mesh zones. During the dynamic transition process, the wing is simulated by adding rotating superimposed translational motion to the wing mesh zone. The rotor is still modeled as virtual disk, and the dynamic transition of rotor is simulated by adding motion to the local coordinate system of virtual disk and the rotor disk mesh zone.

The dynamic transition from 60° to 0° tilt angle is calculated. Firstly, the unsteady calculation of two dynamic tilting processes with transition time of 10 s and 1 s is carried out. The time step number in calculation is set to 1 000, and the inside iteration number in each time step is set to 20. The flight parameters in Table 1 are simplified in the calculation. The tilting motion is set to constant tilting speed, the flight speed variation is simplified by linear fitting, and the rotor collective control variation is simplified by cubic polynomial fitting, and the motion of wing flap is ignored. Then, the quasi-steady calculation of different tilt angles is carried out with the same flight parameters in the dynamic transition process.

Figs.29, 30 show the comparison of unsteady and quasi-steady results of wing lift and rotor thrust respectively. It can be seen that, the unsteady rotor aerodynamic force in dynamic tilting processes at different transition time is consistent with the quasi-steady result. For wing lift, the difference between the quasi-steady result and the unsteady result at transition time of 10 s is still little. The unsteady wing lift at transition time of 1 s is somewhat smaller than the quasi-steady results, and this is due to the flow reattachment delay in the wing tilting motion. In fact, the transition time of a tilt-rotor aircraft is generally more than 10 s, which is much longer than the rotor rotation period, so the unsteady

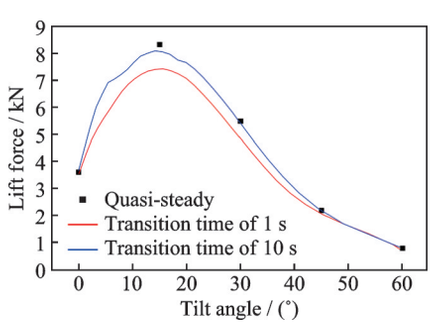

Fig.29 Comparison of wing lift in dynamic transition process with quasi-steady result

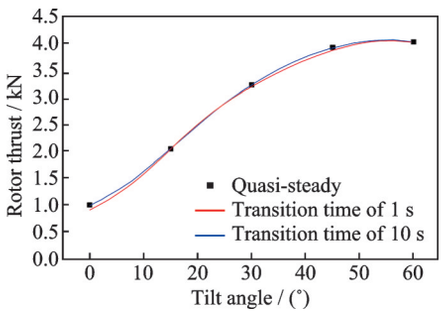

Fig.30 Comparison of rotor thrust in dynamic transition process with quasi-steady result

effect caused by dynamic transition is weak. Tran et al.[30] of NASA carried out comparative calculations of quasi-steady and transient aerodynamic characteristics for the transition state of XV-15 tilt-rotor aircraft. Results show that the variation of rotor and wing aerodynamic force calculated by the two methods are similar, which is consistent with the result in this paper.

3 Conclusions

In this paper, the aerodynamic characteristics of tandem tilt-wing and distributed multi-rotor at different tilt angles are calculated using the virtual disk modeling CFD method. The influence of aerodynamic interaction between front wing, rear wing, front rotors and rear rotors is analyzed.

(1) The virtual disk modeling CFD method is validated using results of rotor-fuselage interaction experiment by Leishman, and the computational and experimental results agree well, which shows the CFD method used in this paper can effectively capture aerodynamic interaction features.

(2) The aerodynamic interaction of the front rotors will obviously increase the front wing lift at different tilt angles. For the computation in this paper, the lift of wing can be increased by more than 40% compared with isolate wing at tilt angle of 15°. This is mainly caused by two factors due to multi-rotor interaction: increasing the wing's velocity magnitude and improving the flow separation of wing at high angles of attack.

(3) For the rear wing, the lift increment caused by aerodynamic interaction is lower than that of front wing at small tilt angle, and the wing lift even decreases at 0° tilt angle, which is mainly due to the influence of downward induced velocity of the front wing. After 30° tilt angle, the lift increment of the rear wing caused by aerodynamic interaction is higher than that of the front wing, and this is because both front and rear rotor slipstreams can improve the flow separation of the rear wing, thus generating larger lift increment.

(4) The front rotor thrust is increased due to the blocking effect of the front wing, especially near the tilt angles of 30° and 45°, and the rotor thrust can be increased by 5.6% at tilt angle of 45°.

(5) For the rear rotor, the aerodynamic interaction does not significantly increase the rotor thrust, and this is because that the axial induced velocity of the front rotor and the downward induced velocity of the front wing decreases the rotor thrust unlike the wing blocking effect.

(6) The aerodynamic force of rotor and wing at different angles calculated by quasi-steady method has few difference with the unsteady results in dynamic tilting process, so the interaction characteristics of tandem tilt-wing and multi-rotor analyzed at fixed tilt angle can be adopted to dynamic tilting condition.

References

[1] DENG Jinghui. Development and prospect of helicopter technology[J]. Aeronautical Science & Technology, 2020, 32(1): 10-16. (in Chinese)

[2] YUAN Mingchuan, LIU Pingan, FAN Feng, et al. Wind tunnel test investigation of coaxial rigid rotor aerodynamic[J]. Journal of Nanjing University of Aeronautics & Astronautics, 2019, 51(2): 257-262. (in Chinese)

[3] FREDERICKS W J, MCSWAIN R G, BEATON B F, et al. Greased Lightning (GL-10) flight testing campaign: NASA-TM—2017-219643[R]. [S.l.]: NASA, 2017: 1-25.

[4] DROANDI G, SYAL M, BOWER G. Tiltwing multi-rotor aerodynamic modeling in hover, transition and cruise flight conditions[C]//Proceedings of the AHS International 74th Annual Forum &Technology Display. Phoenix: AHS, 2018.

[5] GARCIA A J, BARAKOS G N. CFD simulations on the ERICA tiltrotor using HMB2[C]//Proceedings of the 54th AIAA Aerospace Sciences Meeting. San Diego, California, USA: AIAA, 2016.

[6] ZHAO Qijun, NI Tongbing, LI Peng, et al. Experi-

ment on flow mechanism and aerodynamic interaction characteristics of tilt-rotor aircraft[J]. Journal of Aerospace Power, 2018, 33(12): 2900-2912. (in Chinese)

[7] LIM J W. Fundamental investigation of proprotor and wing interactions in tiltrotor aircraft[C]//Proceedings of the VFS 75th Annual Forum & Technology Display. Pennsylvania, USA: [s.n.], 2019.

[8] LI Shangbin, LIN Yongfeng, FAN Feng. The research of aerodynamic characteristics of tilt rotor using wind tunnel and numerical simulation methods[J]. Engineering Mechanics, 2018, 35(5): 249-256. (in Chinese)

[9] LIU Jiahao, LI Gaohua, WANG Fuxin. Calculation analysis of rotor-wing aerodynamic interference characteristics in conversion mode[J]. Acta Aeronautica et Astronautica Sinica, 2022, 43(7): 1-12. (in Chinese)

[10] APPLETON W, FILIPPONE A, BOJDO N. Interaction effects on the conversion corridor of tiltrotor aircraft[J]. The Aeronautical Journal, 2021, 125(1294): 2065-2086.

[11] WU Weiwei, MA Cunwang, ZHANG Lian, et al. Numerical simulation of continuous tilting transition of tiltrotor aircraft[J]. Advances in Aeronautical Science and Engineering, 2021, 12(3): 55-64. (in Chinese)

[12] WU Zhenlong, LI Can, CAO Yihua. Numerical simulation of rotor-wing transient interaction for a tiltrotor in the transition model[J]. Mathematics, 2019, 116(7): 1-18.

[13] BAIN J, MIKI G V, STOLL A. Aerodynamic and acoustic design of the Joby Aviation eVTOL propeller[C]//Proceedings of the Vertical Flight Society's 77th Annual Forum and Technology Display: The Future of Vertical Flight. [S.l.]: VFS, 2021.

[14] STOLL A, BEVIRT J. Development of eVTOL aircraft for urban air mobility at Joby Aviation[C]//Proceedings of the Vertical Flight Society's 78th Annual Forum and Technology Display. Texas: VFS, 2022.

[15] THAI A, BAIN J, MIKIC J V, et al. Flyover noise computations of the Joby Aviation aircraft[C]//Proceedings of the Vertical Flight Society's 79th Annual Forum and Technology Display. West Palm Beach: VFS, 2023.

[16] ROGET B, SITARAMAN J, LIM J, et al. Multi-fidelity investigation of aerodynamics and acoustics of the Joby Aviation aircraft using CREATETM AV Helios[C]// Proceedings of the Vertical Flight Society's 80th Annual Forum and Technology Display. Montreal: VFS, 2024.

[17] PEREZ D G, DIAZ P V, AHMAD A, et al. A comparison of rotor disk modeling and blade-resolved CFD simulations for NASA's tiltwing air taxi[C]//Proceedings of the Vertical Flight Society's 79th Annual Forum and Technology Display. West Palm Beach: VFS, 2023.

[18] PEREZ D G, DIAZ P V, SANGUINETTI A, et al. Tiltwing transition flight analysis using high-fidelity CFD[C]//Proceedings of the Vertical Flight Society's 80th Annual Forum and Technology Display. Montreal: VFS, 2024.

[19] LIU Zeyu. Flight dynamical modeling of a new configuration unmanned tilt-rotor aircraft based on CFD method[D]. Nanjing: Nanjing University of Aeronautics and Astronautics, 2021. (in Chinese)

[20] VERWEIJ A P. An investigation in actuator disc CFD solution applicability for aeroacoustic analysis of propellers and rotors[C]//Proceedings of the 66th American Helicopter Society Forum. Phoenix: AHS, 2010.

[21] CHEN M T, HUBNER J P. Experimental and analytical analysis of rotor-wing Interaction in hover for low Reynolds number flow[J]. Journal of Aerospace Engineering, 2021, 34(6): 1-12.

[22] ZUO Qingyu, XU Guohua, SHI Yongjie. Shipborne helicopter operational limits calculation based on CFD method[J]. Journal of Nanjing University of Aeronautics & Astronautics, 2024 ,56(2): 227-233. (in Chinese)

[23] ZHAO Yanyu, LI Xin, SHI Yongjie, et al. Analysis on rotor-propellers interaction flowfield for compound double-thust-propeller high-speed helicopters[J]. Journal of Nanjing University of Aeronautics & Astronautics, 2017, 49(2): 154-164. (in Chinese)

[24] KAUL U, AHMAD J. Skin friction predictions over a hovering tilt-rotor blade using OVERFLOW2[C]// Proceedings of the 29th AIAA Applied Aerodynamics Conference. Honolulu: AIAA, 2011.

[25] WEKESA D W, WANG C, WEI Y, et al. A numerical analysis of unsteady inflow wind for site specific vertical axis wind turbine: A case study for Marsabit and Garissa in Kenya[J]. Renew Energy, 2015, 76: 648-661.

[26] YOON S, PULLIAM T H, CHADERJIAN N M. Simulations of XV-15 rotor flows in hover using overflow[C]//Proceedings of the Fifth Decennial AHS Aeromechanics Specialists' Conference. San Francisco: AHS, 2014.

[27] WEKESA D W, WANG C, WEI Y, et al. Analytical and numerical investigation of unsteady wind for enhanced energy capture in a fluctuating free-stream[J]. Energy, 2017, 121(15): 854-864.

[28] BI N P, LEISHMAN J D. Experimental study of ro-

tor/body aerodynamic interactions[J]. Journal of Aircraft, 1990, 27(9): 779-788.

[29] RAND O, GESSOW A. Model for investigation of helicopter fuselage influence on rotor flowfields[J]. Journal of Aircraft, 1988, 26(5): 401-402.

[30] TRAN S A, YEO H. Transient and quasi-steady numerical simulations of tiltrotor conversion maneuvers[C]//Proceedings of the Vertical Flight Society's 77th Annual Forum and Technology Display. Texas: VFS, 2022.

Acknowledgement This work was supported by the National Key Laboratory of Helicopter Aeromechanics Fund (No.2024-CXPT-GF-JJ-093-05).

Authors

The first author Prof. **DENG Jinghui** received his Ph.D. degree in aircraft design from Nanjing University of Aeronautics and Astronautics, China, in 2009. He worked as the chief engineer of China Helicopter Research and Development Institute (CHRDI), and currently serves as the chief technical expert in the Aviation Industry Corporation of China (AVIC). He has been primarily engaged in research on rotorcraft key technologies and has received multiple technological achievement awards above the ministerial level, including the Special Award and First Prize of the National Defense Science and Technology Progress Award. His research interests focus on aerodynamic and conceptual design of rotorcraft.

The corresponding author Mr. **YUAN Mingchuan** received his master's degree in aeronautical engineering from Nanjing University of Aeronautics and Astronautics, China, in 2013. He currently works as a senior engineer at China Helicopter Research and Development Institute (CHRDI). His research has focused on aerodynamic interaction , aeroacoustic control and airfoil design of rotorcraft.

Author contributions Prof. **DENG Jinghui** led the entire research for this paper, oversaw the completion of the research program, research methods and research results. Mr. **YUAN Mingchuan** contributed to the analysis of aerodynamic interaction influence on rotor force of the study. Prof. **HUANG Shuilin** contributed to the discussion and background of the study. Mr. **SUN Huixun** contributed to partial computation of the study. Mr. **ZhANG Zihan** contributed to preparation of charts and figures. All authors commented on the manuscript draft and approved the submmion.

Competing interests The authors declare no competing interests.

(Production Editor: SUN Jing)

纵列式倾转机翼和多旋翼在过渡状态下的气动干扰研究

邓景辉，袁明川，黄水林，孙会迅，张子瀚

（中国直升机设计研究所直升机动力学全国重点实验室，景德镇 333000，中国）

摘要：纵列式倾转机翼和多旋翼之间的复杂气动干扰直接影响机翼表面流动和旋翼拉力，是该种构型旋翼飞行器倾转过渡过程中的关键影响因素。为此，采用基于虚拟作用盘模型的CFD方法对该种干扰特性进行了研究，通过向Navier-Stokes方程中添加动量源项来模拟多旋翼的气动效应，在保证气动干扰计算精度的同时有效降低了计算成本。对比分析了有无气动干扰情况下，不同倾转角度时纵列式倾转机翼与多旋翼的气动力及相应流场变化，并比较了动态倾转过渡与固定倾转角状态下的气动力差异。结果表明：多旋翼的气动干扰在不同倾转角度下均明显增加了前倾转机翼的升力，在本文计算的15°倾转角工况下，多旋翼干扰下的机翼升力较孤立机翼提升了40%以上，这与多旋翼干扰引起的来流速度增加及翼面流动分离抑制有关；同时，机翼的阻塞效应会增大旋翼拉力，尤其在30°和45°倾转角附近更为显著；受前机翼下洗流影响，气动干扰对后机翼升力与后旋翼拉力的增加作用并不明显；动态倾转的非定常效应对气动干扰影响较小，动态倾转过渡过程中的旋翼和机翼气动力与固定倾转角状态相差不大。

关键词：气动干扰；纵列式；倾转机翼；多旋翼；过渡状态

研究亮点：

1. 建立了基于分布式虚拟作用盘模型的CFD方法，实现了对纵列式倾转机翼与多旋翼复杂干扰流场的高效数值模拟。

2. 研究发现：多旋翼气动干扰通过增加来流速度及抑制流动分离可有效提升倾转机翼升力，在特定倾角下可使升力提升40%以上；动态倾转过程中的非定常效应对气动干扰影响较小，其瞬时气动力与对应固定倾转角状态相差不大。